

# Qubit-oscillator systems in the ultra-strong coupling regime and their potential for preparing non-classical states

S. Ashhab<sup>1,2</sup> and Franco Nori<sup>1,2</sup>

<sup>1</sup>*Advanced Science Institute, The Institute of Physical and Chemical Research (RIKEN), Wako-shi, Saitama 351-0198, Japan*

<sup>2</sup>*Physics Department, Michigan Center for Theoretical Physics, The University of Michigan, Ann Arbor, Michigan 48109-1040, USA*

(Dated: January 26, 2023)

We consider a system composed of a two-level system (i.e. a qubit) and a harmonic oscillator in the ultra-strong coupling regime, where the coupling strength is comparable to the qubit and oscillator energy scales. Special emphasis is placed on the possibility of preparing non-classical states in this system. These non-classical states include squeezed states, Schrödinger-cat states and entangled states. We start by comparing the predictions of a number of analytical methods that can be used to describe the system under a number of different assumptions, thus analyzing the properties of the system in a number of different parameter regimes. We then examine the ground state of the system and analyze the non-classical properties of this state. We finally discuss some questions related to the possible experimental observation of the non-classical states and the effect of decoherence.

## I. INTRODUCTION

The two-level system (or qubit) and the harmonic oscillator are the two most basic, and perhaps most often studied, components of physical systems. The paradigm of a qubit coupled to a harmonic oscillator has also been analyzed by numerous authors over the past few decades [1, 2]. Physical systems that can be described by this model include natural atoms coupled to optical cavities [2], superconducting qubits coupled to superconducting resonators [4, 5, 6], quantum dots or Cooper-pair boxes coupled to nanomechanical resonators [7, 8, 9] and electrons interacting with phonons in a solid [10].

In the early work on cavity quantum electrodynamics (QED) in atomic systems, the achievable atom-cavity coupling strengths were smaller than the atomic and cavity decay rates, usually limiting observations to only indirect signatures of the theoretically predicted phenomena. Recently, the strong-coupling regime, where the coupling strength is larger than the decay rates in the system, has been achieved [3]. In addition to atomic systems, the strong-coupling regime has been achieved in superconducting circuit-QED systems [4, 5], and superconducting-qubit-nanomechanical-resonator systems are approaching this regime [8]. In fact, superconducting systems are suited for achieving the so-called ultra-strong coupling regime, where the qubit-oscillator coupling strength is comparable to the qubit and oscillator energy scales [15]. One can expect to find new phenomena in this regime that are not present in the weak or moderately strong coupling regimes. Indeed there have been a number of theoretical studies on this system analyzing some of its rich static and dynamical properties [16, 17, 18, 19, 20].

One reason why superconducting systems are well suited for the implementation of qubit-oscillator experiments is the versatility of these systems. For example, in the two earliest experiments on circuit QED, Chiorescu *et al.* [4] employed a low-frequency oscillator, while Wallraff *et al.* [5] implemented a resonant qubit-oscillator system.

Sub-gigahertz qubits have also been realized in recent experiments [11], and there should be no difficulty in fabricating high-frequency oscillators. Therefore, all possible combinations of qubit and oscillator frequencies are accessible, in principle. One advantage of superconducting qubits over natural atoms is the additional control associated with the tunability of essentially all the qubit parameters [14], as will be discussed in more detail below. This tunability contrasts with the situation encountered with natural atoms, where the atomic parameters are essentially fixed by nature. This advantage can be seen clearly in the recent experiments where Fock states and arbitrary oscillator states were prepared in a superconducting qubit-oscillator system [12, 13]. We shall see, however, that the additional controllability comes at the price of having to deal with additional coupling channels to the environment, and this unwanted coupling can increase the fragility of non-classical states.

In this paper we present analytical arguments and numerical calculations of the strongly-coupled qubit-oscillator system from the point of view of the potential for preparing non-classical states in this setup. These states include squeezed states or superpositions of macroscopically distinct states (i.e. Schrödinger-cat state) in the oscillator, as well as qubit-oscillator entangled states. In this study, we shall consider all the different combinations of qubit and oscillator frequencies. We shall also analyze in some detail the effect of the tunability in the qubit parameters on the behaviour of the system.

The paper is organized as follows: In Sec. II we introduce the Hamiltonian that we shall use throughout the paper. In Sec. III we discuss a number of analytical methods that can be used to study the system under a number of different assumptions, and we compare the predictions of these methods. In Sec. IV we present results of numerical calculations that demonstrate the properties of the energy eigenstates of the system, including the non-classical properties of the ground state. In Sec. V we discuss the possibility of preparing and de-

tecting the three types of non-classical states of interest. In Sec. VI we discuss the effect of decoherence on the robustness of non-classical states. Section VII contains some concluding remarks.

## II. HAMILTONIAN

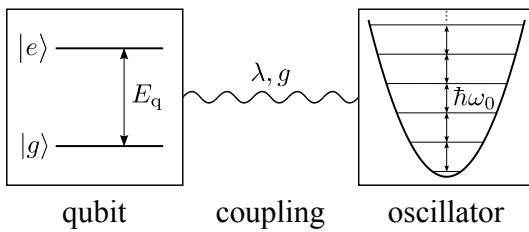


FIG. 1: Schematic diagram of the system under consideration. A qubit with energy separation  $E_q$  between its ground and excited states ( $|g\rangle$  and  $|e\rangle$ ) is coupled to a harmonic oscillator with characteristic frequency  $\omega_0$ . The coupling strength is given by  $g$  or  $\lambda$ , depending on the language used to describe the oscillator.

The system that we consider here is a qubit coupled to a harmonic oscillator, as illustrated in Fig. 1. Rather than worry about deriving the model from a microscopic description of an electric circuit (see e.g. Refs. [15, 22, 23]), we shall assume that the description of the system as being composed of these two physical components with a coupling term of the standard form is an accurate description of the system.

The Hamiltonian of the system is given by:

$$\hat{H} = \hat{H}_q + \hat{H}_{ho} + \hat{H}_{int}, \quad (1)$$

where

$$\begin{aligned} \hat{H}_q &= -\frac{\Delta}{2}\hat{\sigma}_x - \frac{\epsilon}{2}\hat{\sigma}_z \\ \hat{H}_{ho} &= \frac{\hat{p}^2}{2m} + \frac{1}{2}m\omega_0^2\hat{x}^2 \\ \hat{H}_{int} &= g\hat{x}\hat{\sigma}_z, \end{aligned} \quad (2)$$

$\hat{\sigma}_x$  and  $\hat{\sigma}_z$  are the usual Pauli matrices (with  $\hat{\sigma}_z|\uparrow\rangle = |\uparrow\rangle, \hat{\sigma}_z|\downarrow\rangle = -|\downarrow\rangle$ ), and  $\hat{x}$  and  $\hat{p}$  are the position and momentum operators of the harmonic oscillator. The parameters  $\Delta$  and  $\epsilon$  are the gap and bias which characterize the qubit,  $m$  is the oscillator's effective mass,  $\omega_0$  is the oscillator's characteristic frequency, and  $g$  is the qubit-oscillator coupling strength. Note that in contrast to atomic cavity QED systems, where  $\epsilon = 0$ , this parameter is easily tunable in present-day experiments using superconducting qubits. We shall therefore treat  $\epsilon$  as a tunable parameter. For definiteness, we shall take  $\Delta$  and  $g$  to be positive.

It is convenient for some calculations to express the oscillator Hamiltonian using the creation ( $\hat{a}^\dagger$ ) and annihilation ( $\hat{a}$ ) operators:

$$\hat{a} = \hat{X} + i\hat{P}$$

$$\begin{aligned} \hat{a}^\dagger &= \hat{X} - i\hat{P} \\ \hat{X} &= \sqrt{\frac{m\omega_0}{2\hbar}}\hat{x} \\ \hat{P} &= \frac{1}{\sqrt{2\hbar m\omega_0}}\hat{p}, \end{aligned} \quad (3)$$

which give

$$\begin{aligned} \hat{H}_{ho} &= \hbar\omega_0\hat{a}^\dagger\hat{a} + \frac{1}{2}\hbar\omega_0 \\ \hat{H}_{int} &= \lambda(\hat{a} + \hat{a}^\dagger)\hat{\sigma}_z \\ \lambda &= g\sqrt{\frac{\hbar}{2m\omega_0}}. \end{aligned} \quad (4)$$

The coupling strength can therefore be quantified either through  $g$  or  $\lambda$ .

We shall refer to the eigenstates of  $\hat{H}_q$  as the qubit's ground and excited states, denoted by  $|g\rangle$  and  $|e\rangle$ , keeping in mind the caveat that this identification becomes less meaningful for strong qubit-oscillator coupling. The energies of these two states are  $\pm E_q/2$ , where  $E_q = \sqrt{\Delta^2 + \epsilon^2}$ . It is also useful to define an angle  $\theta$  that characterizes the relative size of the  $\hat{\sigma}_x$  and  $\hat{\sigma}_z$  terms in the qubit Hamiltonian:  $\tan\theta = \Delta/\epsilon$ . The eigenstates of  $\hat{H}_{ho}$  are given by  $|n\rangle$ , where  $n = 0, 1, 2, \dots$ , with energies given by  $\hbar\omega_0n$  (up to the ground state energy  $\hbar\omega_0/2$ , which we ignore from now on). The integer  $n$  represents the number of excitations, to which we shall refer as photons, in the oscillator.

## III. COMPARISON BETWEEN DIFFERENT ANALYTICAL METHODS

In this section we describe some analytical methods that can be used to determine the properties and behaviour of the system based on different assumptions (which are valid in different parameter regimes), and we compare the predictions of the different methods.

### A. Weak coupling

The simplest limit is probably the weak-coupling limit [2], where  $\lambda \ll E_q, \hbar\omega_0$ . Strictly speaking, one also needs to consider the number of photons in the oscillator when determining whether the weak-coupling condition is satisfied. However, since in this paper we focus on a system that remains close to its ground state, we assume a small number of photons in the oscillator. In the weak-coupling limit, one can think of the qubit and oscillator as being well-defined, separate physical systems that interact weakly and can exchange excitations with one another [1].

In the limit of small  $\lambda$ , one can treat  $\hat{H}_{int}$  as a small perturbation in the total Hamiltonian. The energy eigenstates in the absence of this perturbation are given by

$|n, g\rangle = |n\rangle \otimes |g\rangle$  and  $|n, e\rangle = |n\rangle \otimes |e\rangle$ , with energies  $\hbar\omega_0 \pm E_q/2$  (ignoring the  $\hbar\omega_0/2$  term in the oscillator's energy).

When there are no degeneracies in the non-interacting system (i.e. in the Hamiltonian given by  $\hat{H}_q + \hat{H}_{ho}$ ), the addition of the perturbation  $\hat{H}_{int}$  has only a small effect on the behaviour of the system. This perturbation only slightly modifies the energy levels and eigenstates of the Hamiltonian.

When  $E_q \approx \hbar\omega$ , the states  $|n, g\rangle$  and  $|n-1, e\rangle$  are nearly degenerate (note that there are an infinite number of such pairs), and the perturbation term couples them. In particular, the relevant matrix elements are given by  $\langle n, g | \hat{H}_{int} | n-1, e \rangle = \lambda\sqrt{n} \sin\theta$ ,  $\langle n, g | \hat{H}_{int} | n, g \rangle = \langle n-1, e | \hat{H}_{int} | n-1, e \rangle = 0$  and  $\langle n-1, e | (\hat{H}_q + \hat{H}_{ho}) | n-1, e \rangle - \langle n, g | (\hat{H}_q + \hat{H}_{ho}) | n, g \rangle = E_q - \hbar\omega_0$ . In other words the effective Hamiltonian that one needs to consider is given by

$$\hat{H}_{\text{eff}} = \begin{pmatrix} \delta/2 & \lambda\sqrt{n} \sin\theta \\ \lambda\sqrt{n} \sin\theta & -\delta/2 \end{pmatrix}, \quad (5)$$

where  $\delta = E_q - \hbar\omega_0$ . Using this Hamiltonian, one can analyze the behaviour of the system. In particular, when  $E_q = \hbar\omega$ , an excitation oscillates back and forth between the qubit and oscillator with frequency  $2\lambda\sqrt{n} \sin\theta$ , which is commonly referred to as the Rabi frequency.

Degeneracies also occur when  $E_q = k\hbar\omega$ , with  $k$  being any integer. In this case, one can go to higher orders in perturbation theory and obtain analytic, though sometimes cumbersome, expressions describing the properties and dynamics of the system. We shall not go any further in analyzing this situation here.

Note that the same results as the explained above (for the case  $E_q \approx \hbar\omega_0$ ) can be obtained by taking the term  $\hat{H}_{int}$  in the Hamiltonian and replacing it by its rotating-wave-approximation (RWA) form:

$$\hat{H}_{\text{int,RWA}} = \lambda (\hat{a}\hat{\sigma}_+ + \hat{a}^\dagger\hat{\sigma}_-), \quad (6)$$

where  $\hat{\sigma}_\pm$  are the qubit raising and lowering operators ( $\hat{\sigma}_+ |g\rangle = |e\rangle$  etc.). This approximation therefore ignores the terms in  $\hat{H}_{int}$  that are proportional to  $\hat{a}^\dagger\hat{\sigma}_+$  and  $\hat{a}\hat{\sigma}_-$ . These terms would create or annihilate two excitations in the system, thus mixing states that have a large energy separation (assuming  $\lambda \ll E_q, \hbar\omega_0$ ), and energy conservation suppresses such transitions. The RWA leads to a Hamiltonian where the state  $|n, g\rangle$  is coupled only to the state  $|n-1, e\rangle$ , which would lead to exactly the same algebra and results mentioned above. Some of the recent studies on ultra-strong coupling have analyzed the effects of the non-RWA terms on the system dynamics [19, 20].

## B. High-frequency, adiabatically adjusting oscillator

The next limit that we consider is when the oscillator's characteristic frequency  $\omega_0$  is large compared to the

qubit's energy splitting (i.e.  $\hbar\omega_0 \gg E_q$ ) and also compared to the coupling strength ( $\hbar\omega_0 \gg \lambda$ ). In this case one can say that the oscillator remains in its initial energy eigenstate, and this state follows adiabatically any changes in the qubit's state. This case was analyzed theoretically in Refs. [17, 18].

The procedure for adiabatically eliminating the high-frequency oscillator from the problem is straightforward. One starts by noting that the qubit is coupled to the oscillator through the operator  $\hat{\sigma}_z$ . As a result, one can think of the oscillator as always monitoring the qubit observable  $\sigma_z$  and adjusting to be in the instantaneous energy eigenstate that corresponds to that value of  $\sigma_z$  (note here that if the qubit is in a superposition of two different  $\sigma_z$  states, each part of the superposition – with a well-defined value of  $\sigma_z$  – will have the oscillator in the corresponding energy eigenstate).

We therefore start by assuming that the qubit has a well-defined value of  $\sigma_z$ , equal to  $\pm 1$ . The oscillator now feels the effective Hamiltonian (calculated from  $\hat{H}_{ho}$  and  $\hat{H}_{int}$ ):

$$\hat{H}_{\text{ho,eff}} \Big|_{\sigma_z=\pm 1} = \hbar\omega_0 \hat{a}^\dagger \hat{a} \pm \lambda (\hat{a} + \hat{a}^\dagger). \quad (7)$$

This Hamiltonian corresponds simply to the original oscillator Hamiltonian with a constant force term applied to it. This force term can be eliminated using the transformation

$$\hat{a}' = \hat{a} \pm \frac{\lambda}{\hbar\omega_0}, \quad (8)$$

which gives

$$\hat{H}_{\text{ho,eff}} \Big|_{\sigma_z=\pm 1} = \hbar\omega_0 \hat{a}'^\dagger \hat{a}' - \frac{\lambda^2}{\hbar\omega_0}. \quad (9)$$

The above steps can also be carried out in the language of the operators  $\hat{x}$  and  $\hat{p}$ :

$$\begin{aligned} \hat{H}_{\text{ho,eff}} \Big|_{\sigma_z=\pm 1} &= \frac{\hat{p}^2}{2m} + \frac{1}{2}m\omega_0^2 \hat{x}^2 \pm g\hat{x} \\ x' &= x \pm \frac{g}{m\omega_0^2} \\ p' &= p \\ \hat{H}_{\text{ho,eff}} \Big|_{\sigma_z=\pm 1} &= \frac{\hat{p}'^2}{2m} + \frac{1}{2}m\omega_0^2 \hat{x}'^2 - \frac{g^2}{2m\omega_0^2}. \end{aligned} \quad (10)$$

The energy levels of the oscillator are given by  $n\hbar\omega_0 - \lambda^2/(\hbar\omega_0)$ , independently of the qubit's state. There will therefore not be a qubit-state-dependent energy that we need to take into account when we turn to analyzing the behaviour of the (slow) qubit. The oscillator's energy eigenstates, however, are slightly dependent on the state of the qubit. In particular,

$$\langle n_{\sigma_z=+1} | m_{\sigma_z=+1} \rangle = \langle n_{\sigma_z=-1} | m_{\sigma_z=-1} \rangle = \delta_{nm}, \quad (11)$$

and

$$\langle n_{\sigma_z=+1} | m_{\sigma_z=-1} \rangle = \begin{cases} e^{-2\lambda^2/(\hbar\omega_0)^2} \left(-\frac{2\lambda}{\hbar\omega_0}\right)^{m-n} \sqrt{\frac{n!}{m!}} L_n^{m-n} \left[ \left(\frac{2\lambda}{\hbar\omega_0}\right)^2 \right], & m \geq n \\ e^{-2\lambda^2/(\hbar\omega_0)^2} \left(\frac{2\lambda}{\hbar\omega_0}\right)^{n-m} \sqrt{\frac{m!}{n!}} L_m^{n-m} \left[ \left(\frac{2\lambda}{\hbar\omega_0}\right)^2 \right], & m < n, \end{cases} \quad (12)$$

where  $\delta_{nm}$  is the Kronecker delta, and  $L_i^j$  are the associated Laguerre polynomials.

Having obtained the states of the high-frequency oscillator and the properties of these states, one can now turn to the slow part of the system, namely the qubit. We need to construct a renormalized Hamiltonian, which will be a  $2 \times 2$  matrix (assuming here that the index  $n$  of the oscillator's state is specified). The four relevant matrix elements can be calculated straightforwardly as

$$\begin{aligned} \langle \widetilde{n, \uparrow} | \hat{H}_q | \widetilde{n, \uparrow} \rangle &= -\langle \widetilde{n, \downarrow} | \hat{H}_q | \widetilde{n, \downarrow} \rangle = -\frac{\epsilon}{2} \\ \langle \widetilde{n, \uparrow} | \hat{H}_q | \widetilde{n, \downarrow} \rangle &= \langle \widetilde{n, \downarrow} | \hat{H}_q | \widetilde{n, \uparrow} \rangle \\ &= -\frac{\Delta}{2} e^{-2\lambda^2/(\hbar\omega_0)^2} L_n^0 \left[ \left(\frac{2\lambda}{\hbar\omega_0}\right)^2 \right] \end{aligned} \quad (13)$$

and all other matrix elements are negligibly small. Note that we are using the tildes in order to emphasize that the states in this subsection are different from the direct product states of Sec. III A.

The exponential and Laguerre-function factors are both slightly smaller than one for small values of  $\lambda/(\hbar\omega_0)$ . The qubit therefore experiences a small reduction in the coupling (or ‘tunnelling’) between the states  $|\uparrow\rangle$  and  $|\downarrow\rangle$  in the weak-coupling limit ( $\lambda \ll \hbar\omega_0$ ). Note that this decrease in the renormalized value of  $\Delta$  depends on the number of photons in the oscillator, which can lead to beating dynamics and other interesting phenomena [17, 18].

If we keep increasing  $\lambda/(\hbar\omega_0)$ , without worrying about satisfying the validity condition of the present approximation, we find that the Laguerre polynomial and therefore the renormalized qubit gap vanish at  $n$  different  $\lambda/(\hbar\omega_0)$  values. At these points, the states  $|\widetilde{n, \uparrow}\rangle$  and  $|\widetilde{n, \downarrow}\rangle$  are completely decoupled. Apart from these features, the renormalized gap decreases as a Gaussian function with increasing  $\lambda/(\hbar\omega_0)$ . Note that there is no point that can be seen as a ‘critical point’ in this case, in contrast to what happens in the two calculations that we discuss next (in fact, the critical point would be expected to occur within the regime of validity of the present approximation).

### C. High-frequency, adiabatically adjusting qubit

We now take the limit where  $E_q$  is much larger than both  $\hbar\omega_0$  and  $\lambda$ . Similarly to what was done in Sec. III B,

we now say that the qubit remains in the same energy eigenstate (ground or excited state), and this state changes adiabatically following the dynamics of the slow oscillator. We therefore start by finding the energy eigenstates of the (fast-adjusting) qubit for a given state of the (slow) oscillator. Since the interaction between the qubit and the oscillator is mediated by the oscillator's position operator  $\hat{x}$ , we start the calculation by assuming that  $x$  has a well-defined value and treat the effective Hamiltonian (obtained from  $\hat{H}_q$  and  $\hat{H}_{\text{int}}$ ):

$$\hat{H}_{q,\text{eff}}|_x = -\frac{\Delta}{2}\hat{\sigma}_x - \frac{\epsilon}{2}\hat{\sigma}_z + gx\hat{\sigma}_z. \quad (14)$$

The eigenvalues and eigenstates of this Hamiltonian are given by:

$$\begin{aligned} E_{q,1|x} &= -\frac{1}{2}\sqrt{\Delta^2 + (\epsilon - 2gx)^2} \\ |g_x\rangle &= \cos\frac{\varphi}{2}|\uparrow\rangle + \sin\frac{\varphi}{2}|\downarrow\rangle \\ E_{q,2|x} &= \frac{1}{2}\sqrt{\Delta^2 + (\epsilon - 2gx)^2} \\ |e_x\rangle &= \sin\frac{\varphi}{2}|\uparrow\rangle - \cos\frac{\varphi}{2}|\downarrow\rangle \\ \tan\varphi &= \frac{\Delta}{\epsilon - 2gx}. \end{aligned} \quad (15)$$

We can now take these results and use them to analyze the behaviour of the oscillator. We note here that since the variable  $x$  appears in the above expressions, the  $\hat{x}$  and  $\hat{p}$  operators are more suitable for this calculation than the  $\hat{a}$  and  $\hat{a}^\dagger$  operators.

Since the qubit's energy depends on the oscillator's position  $x$ , the oscillator's effective potential now acquires a new contribution (which depends on the qubit's state):

$$V_{\text{eff}}(x) = \frac{1}{2}m\omega_0^2x^2 \pm \frac{1}{2}\sqrt{\Delta^2 + (\epsilon - 2gx)^2}. \quad (16)$$

The plus sign corresponds to the qubit being in the excited state, and the minus sign corresponds to the qubit being in the ground state. In addition to the above effect of the qubit on the oscillator, the qubit's state changes as the oscillator's position changes, and the oscillator's kinetic-energy term will also be modified in principle (this effect is similar to the renormalization of  $\Delta$  encountered in Sec. III B). However, for a sufficiently high-frequency qubit, changes in the qubit's state will be small, and consequently the change in the kinetic energy term can be neglected.

We now note that the effective potential in Eq. (16) is no longer a harmonic potential. The second term describes one of the two branches of a hyperbola, depending on the qubit's state. It will therefore not be possible to derive general analytical results, and we have to start considering some special cases.

In the limit  $E_q \gg g|x|$  for the relevant values of  $x$ , the effective potential in Eq. (16) can be approximated by:

$$\begin{aligned} V_{\text{eff}}(x) &\approx \frac{1}{2}m\omega_0^2x^2 \pm \left( \frac{\sqrt{\Delta^2 + \epsilon^2}}{2} - \frac{\epsilon gx - g^2x^2}{\sqrt{\Delta^2 + \epsilon^2}} \right) \\ &= \frac{1}{2}m\tilde{\omega}_0^2 \left( x \mp \frac{\epsilon g}{m\tilde{\omega}_0^2 E_q} \right)^2 \pm \frac{E_q}{2}, \end{aligned} \quad (17)$$

where

$$\tilde{\omega}_0^2 = \omega_0^2 \pm 2\frac{g^2}{mE_q}. \quad (18)$$

The oscillator's effective potential is modified in two ways depending on the qubit's state. Firstly, the location of the minimum is shifted to the left or right by a distance proportional to  $\epsilon/E_q = \cos\theta$  (This effect is absent when the qubit is biased at the degeneracy point). We pause for a moment here to derive a condition on the system parameters following from the above-mentioned shift in the effective potential. Even in the low-lying energy eigenstates, where we can assume that  $x$  is roughly given by the location of the shifted minimum of the effective potential, if we consider the ‘worst-case scenario’ of  $\cos\theta \sim 1$ , we find that the condition  $E_q \gg g|x|$  reduces to:

$$\frac{g^2}{m\omega_0^2 E_q} \ll 1, \quad (19)$$

or alternatively

$$\frac{\lambda^2}{\hbar\omega_0 E_q} \ll 1. \quad (20)$$

If this condition is not satisfied, one would need to be careful when applying the high-frequency-qubit approximation. Indeed, the above condition turns out to be closely related to the instability condition that we shall discuss shortly.

The other modification to the oscillator's effective potential caused by the coupling to the qubit is the renormalization of the oscillator's frequency. According to Eq. (18), the oscillator's effective frequency is increased for the qubit's excited state and reduced for the qubit's ground state (This phenomenon is the basis of the so-called quantum-capacitance and quantum-inductance qubit-readout techniques [24]). In particular, if one has the situation where the qubit is in its ground state and

$$\frac{2g^2}{m\omega_0^2 E_q} > 1, \quad \text{i.e.} \quad \frac{4\lambda^2}{\hbar\omega_0 E_q} > 1, \quad (21)$$

the renormalized frequency becomes imaginary. This result signals an instability in the system. In particular, it indicates that our expansion of the square-root in Eq. (17) is no longer valid, the reason being that  $x$  would increase indefinitely and the condition  $E_q \gg g|x|$  would be violated.

The instability obtained above would raise questions about the validity of the assumption of an adiabatically adjusting qubit in that case. Nevertheless, we shall not worry about this point now, and we continue the calculation. Instead of the square-root expansion used in Eq. (17), a more suitable effective potential would have the form

$$V_{\text{eff}}(x) = \frac{1}{2}m\omega_0^2x^2 \pm \left| gx - \frac{\epsilon}{2} \right| \quad \text{when} \quad |x| \gg \frac{\Delta}{g}, \frac{|\epsilon|}{g}. \quad (22)$$

This potential is well behaved at  $|x| \rightarrow \infty$ , ensuring the absence of any serious breakdown. We can therefore proceed with the calculation using the effective potential in Eq. (16).

In order to make a few more statements about the case of strong coupling (i.e. above the critical point), it is useful to start with the case  $\epsilon = 0$  and include a finite bias afterwards. When  $\epsilon = 0$ , the oscillator's effective potential takes the form

$$V_{\text{eff}}(x) = \begin{cases} \left( \frac{1}{2}m\omega_0^2 \pm \frac{g^2}{\Delta} \right) x^2 \pm \frac{\Delta}{2} & , x \ll \Delta/g \\ \frac{1}{2}m\omega_0^2 x^2 \pm |gx| & , x \gg \Delta/g \end{cases} \quad (23)$$

For the case with the qubit in its excited state (i.e. when one has the plus signs in the above expressions), the effective potential is a slightly non-harmonic potential, and one can expect the oscillator states to look more or less like the usual harmonic oscillator states. For the case with the qubit in its ground state, and when  $2g^2/(m\omega_0^2\Delta) \ll 1$ , one also has a slightly non-harmonic potential. For the qubit's ground state and  $2g^2/(m\omega_0^2\Delta) > 1$  (this condition indicates crossing the critical point into the bistability region, where the effective potential has two local minima), the oscillator's effective potential is a double well potential. The low-lying oscillator states in this case are quantum superpositions with  $x$  localized around

$$x_0 = \pm \sqrt{\frac{g^2}{m^2\omega_0^4} - \frac{\Delta^2}{4g^2}}. \quad (24)$$

If one goes well beyond the critical point, the above expression reduces to

$$x_0 \approx \pm \frac{g}{m\omega_0^2}, \quad (25)$$

with minimum potential energy

$$V_{\text{min}} \approx -\frac{g^2}{2m\omega_0^2}, \quad (26)$$

and curvature

$$\frac{d^2V_{\text{eff}}}{dx^2} \Big|_{x=x_0} \approx m\omega_0^2. \quad (27)$$

Note that this curvature is identical to that of the free oscillator (i.e. when  $g = 0$ ).

One can use the above results to estimate the energy separation between the ground state and first excited state. These two states will be the symmetric and antisymmetric superpositions of the ground states localized around the two minima in the double-well potential. The distance between the two minima is of the order of Eq. (25), and the height of the energy barrier separating the two minima is given by  $-V_{\text{min}}$  from Eq. (26). Using the WKB formula, one finds that the energy separation between the two lowest states (and also within similar pairs of higher energy levels) is exponential in the parameter  $\sqrt{-mV_{\text{min}}}x_0/\hbar$ , which is proportional to  $g^2/(m\omega_0^3\hbar)$ , or alternatively  $\lambda^2/(\hbar\omega_0)^2$ . This scaling is the same as the one obtained in Sec. III B.

We now introduce  $\epsilon$  to the problem. Far below the critical point, the effect of  $\epsilon$  can be obtained easily from Eq. (17): the location of the minimum in the single-well effective potential is slightly shifted to the left or right. More care is required above the critical point, where one has the double-well effective potential. In this case, a finite value of  $\epsilon$  breaks the symmetry between the left and right wells, thus giving an energetic preference for one of the two wells. In order to localize the energy eigenstates,  $\epsilon$  has to be larger than the energy separation within one of the energy-level pairs discussed above, i.e.  $\epsilon$  needs to be larger than a quantity that is exponentially small in  $g^2/(m\omega_0^3\hbar)$ . Clearly, this localization happens at smaller values of  $\epsilon$  as one goes deeper into the bistability region. This result means that the superpositions involving both wells become increasingly fragile with increasing coupling strength.

Finally we note that above the critical point, one finds that the condition  $E_q \gg g|x|$  can no longer be satisfied for any of the energy eigenstates. Therefore, one might expect that the present approximation cannot be trusted. It turns out, however, that the qualitative results discussed above hold, even when  $\lambda > E_q$ . The reason why the approximation of an adiabatically adjusting qubit is still valid in this case is that even though large changes in the qubit's states can occur in this case, they involve the very slow process of tunnelling between the two wells in the effective potential. The qubit can therefore adjust adiabatically to this slow process.

#### D. Semiclassical calculation

A semiclassical calculation can go as follows (alternative semiclassical calculations can be found in [16, 18]): The five different variables  $x, p, \sigma_x, \sigma_y$  and  $\sigma_z$  are treated as classical variables whose dynamics obeys the Hamiltonian in Eqs. (1) and (2), without the hats. These vari-

ables obey the constraint  $C = \sigma_x^2 + \sigma_y^2 + \sigma_z^2 = 1$ . One can therefore find the ground state relatively easily by minimizing the Hamiltonian under the above constraint. Minimizing the function  $\tilde{H} = H - \mu C$ , with  $\mu$  being a Lagrange multiplier, results in the set of equations

$$\begin{aligned} \frac{d\tilde{H}}{dx} &= m\omega_0^2 x + g\sigma_z = 0 \\ \frac{d\tilde{H}}{dp} &= \frac{p}{m} = 0 \\ \frac{d\tilde{H}}{d\sigma_x} &= -\frac{\Delta}{2} - 2\mu\sigma_x = 0 \\ \frac{d\tilde{H}}{d\sigma_y} &= -2\mu\sigma_y = 0 \\ \frac{d\tilde{H}}{d\sigma_z} &= -\frac{\epsilon}{2} + gx - 2\mu\sigma_z = 0, \end{aligned} \quad (28)$$

which are to be solved under the constraint  $\sigma_x^2 + \sigma_y^2 + \sigma_z^2 = 1$ . The first four equations lead to  $x = -g\sigma_z/(m\omega_0^2)$ ,  $p = 0$ ,  $\mu = -\Delta/(4\sigma_x)$ , and  $\sigma_y = 0$ . The constraint gives  $\sigma_x = \pm\sqrt{1 - \sigma_z^2}$ . One is therefore left with the equation

$$-\frac{\epsilon}{2} - \frac{g^2\sigma_z}{m\omega_0^2} \pm \frac{\Delta\sigma_z}{2\sqrt{1 - \sigma_z^2}} = 0, \quad (29)$$

which can be re-expressed as

$$-\frac{\epsilon}{\Delta} - \left( \frac{2g^2}{m\omega_0^2\Delta} \pm \frac{1}{\sqrt{1 - \sigma_z^2}} \right) \sigma_z = 0. \quad (30)$$

The above equation cannot be solved in closed form, in general. However, one can make some general statements about the solution (see Fig. 2). For the plus sign (Fig. 2a), the second term in Eq. (30) is a monotonically decreasing function that approaches  $+\infty$  when  $\sigma_z \rightarrow -1$  and approaches  $-\infty$  when  $\sigma_z \rightarrow 1$ . There is therefore one solution to the equation in that case. It turns out that this solution does not correspond to the ground state. The ground state is obtained when using the minus sign. In this case, there are three possibilities: The first possibility is to have  $2g^2 < m\omega_0^2\Delta$ . In this case (Fig. 2c), we find that the second term is a monotonically increasing function that approaches  $-\infty$  when  $\sigma_z \rightarrow -1$  and approaches  $+\infty$  when  $\sigma_z \rightarrow 1$ . There is therefore only one solution to Eq. (30). The second and third possibilities for the solutions of Eq. (30) occur when  $2g^2 > m\omega_0^2\Delta$ . In this case (Figs. 2e and 2g), the second term in Eq. (30) develops a local maximum and a local minimum between  $\sigma_z = -1$  and  $\sigma_z = 1$ . Depending on the value of  $\epsilon$ , there can be either one or three solutions. In particular, when  $\epsilon = 0$ , the three solutions are given by  $\sigma_z = 0$ , which turns out to be an unstable stationary point, and  $\sigma_z = \pm\sqrt{1 - (m\omega_0^2\Delta/2g^2)^2}$ , which are two degenerate ground states (it is easy to verify that this result agrees with Eq. 24).

One can intuitively understand the effect of having a finite value of  $\epsilon$  using the language of Sec. III C. For

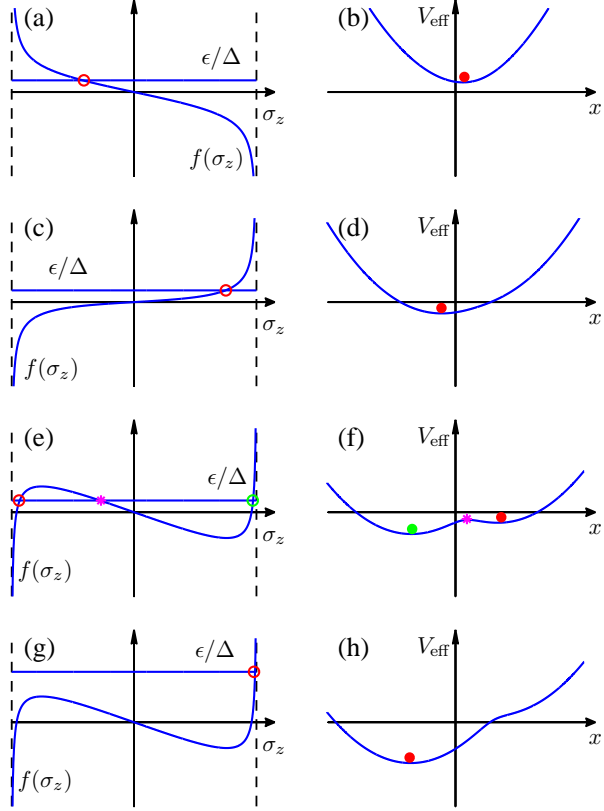


FIG. 2: (Color online) Graphical solution of Eq. (30) [a,c,e,g] and the associated effective potentials from Sec. III C [b,d,f,h] in the different possible cases. The horizontal lines in panels [a,c,e,g] represent the first term in Eq. (30), and the function  $f(\sigma_z)$  is the second term in the equation. The circles in the left panels mark the stable solutions of Eq. (30), and the dots in the right panels mark the minima in the effective potential of Sec. III C, i.e. Eq. (16). The magenta stars in panels (e) and (f) mark an unstable stationary point, i.e. a local maximum. Panels (a) and (b) correspond to the plus signs in Eqs. (16) and (30), and panels (c-h) correspond to the minus signs. In panels (c) and (d), the coupling is below the critical point, i.e.  $2g^2 < m\omega_0^2 E_q$ . In panels (e) and (f), the coupling is above the critical point and  $\epsilon$  is small. In panels (e) and (f), the coupling is above the critical point and  $\epsilon$  is large.

$\epsilon = 0$ , one has an effective trapping potential for the variable  $x$ , and this potential has the shape of a harmonic-oscillator-like single-well potential when  $2g^2 < m\omega_0^2 \Delta$  and a double-well potential when  $2g^2 > m\omega_0^2 \Delta$ . This situation explains the existence of one ground state when  $2g^2 < m\omega_0^2 \Delta$  and two degenerate ground states when  $2g^2 > m\omega_0^2 \Delta$ . The effect of adding  $\epsilon$  to the problem is to create a tilt in the effective trapping potential; a positive value of  $\epsilon$  favours the negative- $x$  solution (here we have in mind the ground-state solution). If the tilt is weak, one has a global ground state in the deeper well and a local minimum in the shallower well. If the tilt exceeds a certain critical value, the shallow well is eliminated, and one recovers a single-well potential.

We make a final note on the fact that we started the calculation by raising a question related to the ground state but found multiple solutions. The reason for this result is the fact that Eq. (28) locates all stationary points, and not only the ground state. We can therefore find high-energy states that are in principle unstable against relaxation to lower-energy states.

### E. Concluding remarks

We conclude this section with some remarks on the predictions of the different analytical methods. The weak-coupling limit is suited for studying the excitation-exchange dynamics between the qubit and oscillator, but it does not give any hint of an instability or strong correlation between the qubit and oscillator. The main result of the adiabatic-oscillator approximation is the renormalized qubit gap. Apart from the oscillatory behaviour in the gap, the Gaussian-function decrease at large  $\lambda/(\hbar\omega_0)$  values is a signature of the strong entanglement between the qubit and the oscillator in the energy eigenstates. Nevertheless, no ‘critical point’, i.e. a point that is associated with a sudden change in any of the effective qubit parameters (particularly the renormalized gap), is obtained in that calculation. The adiabatic-qubit approximation predicts a reduced effective oscillator frequency for weak coupling, and a qualitative change in behaviour upon crossing the critical point

$$\frac{4\lambda^2}{\hbar\omega_0 E_q} > 1. \quad (31)$$

Above the critical point, the energy eigenstates can be highly entangled qubit-oscillator states. As in the adiabatic-oscillator approximation, the separation between neighbouring energy levels is found to follow a Gaussian function dependence in the parameter  $\lambda/(\hbar\omega_0)$ . The adiabatic-oscillator and adiabatic-qubit approximations give different predictions regarding the typical value of  $\lambda$  at which the Gaussian-function decrease in energy separation starts: the former gives  $\lambda \sim \hbar\omega_0$  and the latter gives  $\lambda \sim \sqrt{\hbar\omega_0 \Delta}$ . The semiclassical calculation produces the same critical-point condition as the adiabatic-qubit approximation. Even though the semiclassical calculation naturally cannot produce any entangled-state solutions, its results can be used as a starting point for studying quantum superpositions of the different semiclassical solutions.

## IV. NUMERICAL CALCULATIONS

In this section we present results of numerical calculations that demonstrate the behaviour of the system in the different parameter regimes. In particular, we perform calculations for the near-resonant case, the high-frequency-oscillator case and the high-frequency-qubit

case. In one of the calculations, we also examine the transition between the different regimes.

### A. Energy-level spectrum

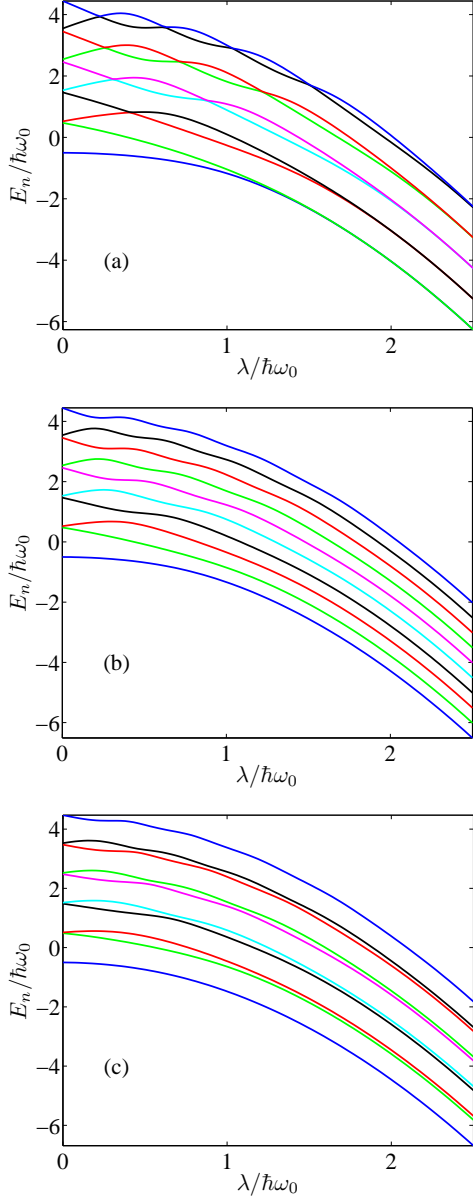


FIG. 3: (Color online) Lowest ten energy levels in the resonant case, i.e. when  $\hbar\omega_0/E_q = 1$ . The re-scaled energy  $E_n/(\hbar\omega_0)$  with  $n = 1, 2, \dots, 10$  is plotted as a function of the re-scaled coupling strength  $\lambda/(\hbar\omega_0)$ . Panels (a), (b) and (c) correspond to  $\theta = 0, \pi/6$  and  $\pi/3$ , respectively [recall that  $\theta = \arctan(\Delta/\epsilon)$ ].

In Fig. 3 we plot the energies of the lowest ten levels as a function of the coupling strength  $\lambda$  in the resonant case  $\omega = E_q$ . When  $\epsilon = \lambda = 0$ , the ground state is non-degenerate and each higher energy level is doubly degen-

erate. The separation between the levels is  $\hbar\omega_0$ , which is also equal to  $E_q$ . As  $\lambda$  increases, the energy levels shift up or down, and several avoided crossings are encountered. In the large  $\lambda$  limit, all energy levels become doubly degenerate (i.e. they form pairs), including the ground state. The separation between the different pairs of energy levels in this limit is again  $\hbar\omega_0$ . These results agree with the picture of the effective double-well potential of Sec. III C. For a small but finite bias  $\epsilon$  (i.e. small but finite  $\theta$ ) and small coupling strength  $\lambda$ , the energy level structure is similar to that in the  $\epsilon = 0$  case, except that the levels do not approach each other as much at the avoided crossings. In the large  $\lambda$  limit, there are no degeneracies: the energy levels are separated by the alternate distances  $\epsilon$  and  $\hbar\omega_0 - \epsilon$ . This structure reflects the small asymmetry in the double-well potential caused by a small tilt. For large  $\theta$ , all features in the spectrum are suppressed, except for the overall decrease in the energy with increasing  $\lambda$ .

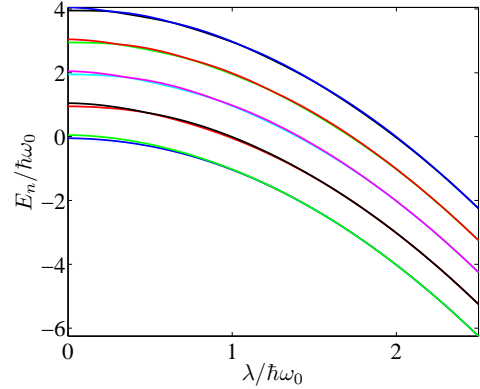


FIG. 4: (Color online) Lowest ten energy levels in the case of a high-frequency oscillator;  $\hbar\omega_0/E_q = 10$ . Here we only show the results for  $\theta = 0$ , because the overall appearance of the plots is independent of  $\theta$ . More details can be seen in Fig. 5.

In Fig. 4 we plot the energies of the lowest ten levels as a function of  $\lambda$  in the case of a high-frequency oscillator, i.e. when  $E_q \ll \hbar\omega_0$ . If one considers a pair of energy levels, e.g. the lowest two energy levels, one has a modified effective qubit Hamiltonian, as explained in Sec. III B. When  $\lambda = 0$ , one recovers the bare qubit Hamiltonian. As  $\lambda$  increases, the effective qubit gap  $\Delta$  decreases and approaches zero in the limit  $\lambda/(\hbar\omega_0) \rightarrow \infty$ . In Fig. 5 we plot the separations within the four lowest pairs of energy levels. We can see that the effective gap follows the shape of the Gaussian function times a Laguerre polynomial, vanishing at the zeros of the Laguerre polynomials. As  $\theta$  is increased from zero, i.e. as the ratio  $\Delta/\epsilon$  decreases, the dependence of the energy-level separation on the coupling strength becomes weaker (this phenomenon can be seen by comparing the different panels in Fig. 5). Note that the location of the peaks does not change; it is simply that the effect of the gap on the energy levels becomes smaller with increasing  $\theta$ .

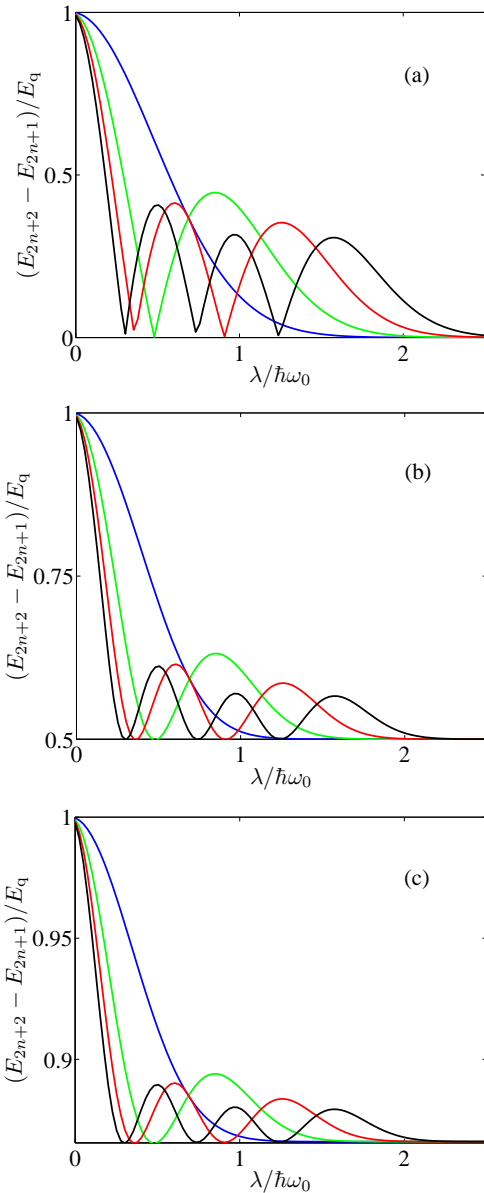


FIG. 5: (Color online) The re-scaled energy separation  $(E_{2n+2} - E_{2n+1})/E_q$  within the lowest four pairs of energy levels [i.e. for  $n = 0$  (blue), 1 (green), 2 (red) and 3 (black)], as a function of  $\lambda/(\hbar\omega_0)$ . As in Fig. 4, we take  $\hbar\omega/E_q = 10$ . In Panels (a), (b) and (c),  $\theta = 0, \pi/6$  and  $\pi/3$ , respectively. Note that the minimum value on the  $y$ -axis is different in the three panels.

In Fig. 6 we plot the energies of the lowest ten energy levels as a function of  $\lambda$  in the case of a high-frequency qubit, i.e. when  $E_q \gg \hbar\omega_0$ . The most dramatic effects occur for  $\theta = 0$ . The ground state energy remains essentially constant between  $\lambda = 0$  and  $\lambda = \sqrt{\hbar\omega_0\Delta}/2$ . Beyond this point the ground state energy decreases indefinitely with increasing  $\lambda$ . Furthermore, below the critical point, the low-lying energy levels approach each other with increasing  $\lambda$  as if they were going to collapse to one

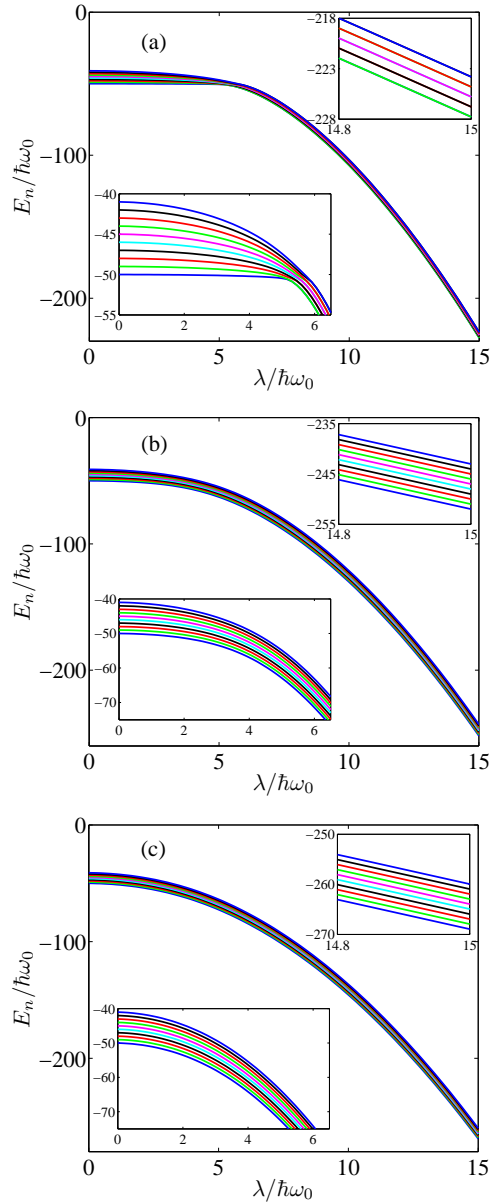


FIG. 6: (Color online) Lowest ten energy levels in the case of a high-frequency qubit;  $\hbar\omega_0/E_q = 0.01$ . In Panels (a), (b) and (c),  $\theta = 0, \pi/6$  and  $\pi/3$ , respectively. The insets show an enlarged view of the weak-coupling and strong-coupling regions.

point, as would be expected for a vanishing  $\tilde{\omega}_0$ . Above the critical point, the energy levels form pairs whose intra-pair separation decreases with increasing  $\lambda$ . The above scenario is suppressed as  $\theta$  is increased. There is no longer any sign of a critical point, and the energy-level separations are independent of  $\lambda$ .

## B. squeezing, entanglement, and ‘cat-ness’ in the ground state

One obvious possibility for the preparation of squeezed, entangled or Schrödinger-cat states in the case of ultra-strong coupling is to have a ground state that exhibits one of these unusual properties. With this point in mind, in this section we analyze the oscillator’s squeezing and cat-ness as well as the qubit-oscillator entanglement in the ground state for a number of different choices of parameters.

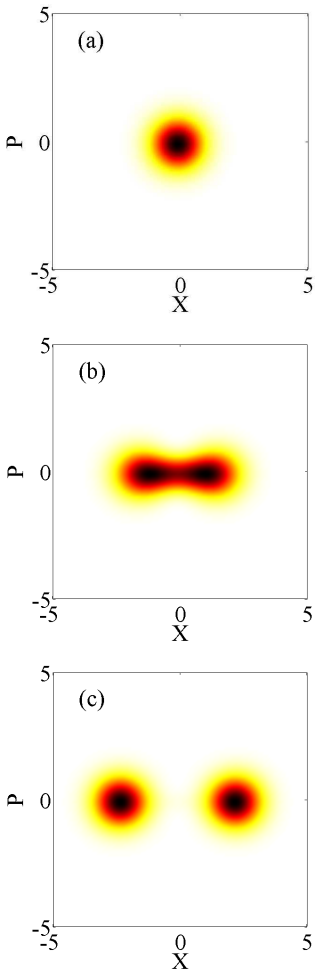


FIG. 7: The  $Q$ -function of the oscillator’s state in the ground state of the combined system. Here we take  $\hbar\omega_0/\Delta = 0.1$  and  $\epsilon = 0$ . The three panels correspond to  $\lambda/(\hbar\omega_0) = 0.5, 2$  and  $2.5$ . For clarity, we adjust the color scheme in the different panels such that the highest point is always black (note that the  $Q$ -function is always normalized to unity). The oscillator’s state goes from a coherent state with no photons (i.e. the vacuum state) in the absence of coupling, to a squeezed state for low to moderate coupling strengths and then to a qubit-oscillator entangled state in the strong-coupling regime (note that the  $Q$ -function does not distinguish between an unentangled cat state in the oscillator and a qubit-oscillator entangled state; however, we shall show below that the situation in panel (c) corresponds to an entangled state).

As a first step, we plot the  $Q$ -function of the oscillator’s state in the ground state of the coupled system,

$$Q(X, P) = \frac{1}{\pi} \langle X + iP | \rho_{\text{osc}} | X + iP \rangle, \quad (32)$$

where  $\rho_{\text{osc}}$  is the oscillator’s reduced state after tracing out the qubit from the ground state,  $\rho_{\text{osc}} = \text{Tr}_q\{|\Psi_{\text{GS}}\rangle\langle\Psi_{\text{GS}}|\}$  with  $|\Psi_{\text{GS}}\rangle$  being the ground state of the combined system, and the coherent states in the above formula are given by

$$|\alpha\rangle = \exp\{\alpha\hat{a}^\dagger - \alpha^*\hat{a}\} |0\rangle. \quad (33)$$

The state  $|0\rangle$  represents the vacuum state with the oscillator in its ground state. The  $Q$ -function for a sequence of  $\lambda$  values is shown in Fig. 7.

Going beyond the pictorial description shown above, a quantifier for both the squeezing and cat-ness of the oscillator’s state is the set of two squeezing parameters in the  $x$  and  $p$  quadratures as well as the product of the quadrature variances (note here that the oscillator’s state is always mirror-symmetric with respect to the  $x$  axis in the setup under consideration, giving  $\langle\hat{p}\rangle = 0$ ). After the appropriate conversion into dimensionless variables, these quantifiers are given by

$$\begin{aligned} s_x &= 4 \left\langle \left( \hat{X} - \langle \hat{X} \rangle \right)^2 \right\rangle - 1 \\ s_p &= 4 \left\langle \left( \hat{P} - \langle \hat{P} \rangle \right)^2 \right\rangle - 1 \\ K &= \left\langle (\hat{x} - \langle \hat{x} \rangle)^2 \right\rangle \left\langle (\hat{p} - \langle \hat{p} \rangle)^2 \right\rangle \\ &= \frac{\hbar^2}{4} (1 + s_x)(1 + s_p). \end{aligned} \quad (34)$$

The parameter  $K$  is equal to  $\hbar^2/4$  for a minimum-uncertainty state (including both coherent and quadrature-squeezed states) and is larger than that lower bound for any other state (including Schrödinger-cat and qubit-oscillator entangled states). In Fig. 8 we plot the momentum squeezing parameter as a function of the coupling strength  $\lambda$ . In the weak-coupling regime, the squeezing increases with increasing  $\lambda$ . However, as one enters the strong-coupling regime and the ground state becomes more and more entangled, the squeezing is lost. The maximum achievable squeezing is largest for the case of a high-frequency qubit,  $\hbar\omega \ll \Delta$ . Indeed, as explained in Sec. III C, the oscillator’s effective potential becomes flatter and flatter as one approaches the critical point, leading to a momentum squeezing parameter close to  $-1$ .

As  $|s_p|$  increases, one can ask whether the oscillator’s state is a quadrature-squeezed, minimum-uncertainty state or it deviates from this ideal squeezed state. The answer to this question can be obtained by analyzing the parameter  $K$ . We do not show any plots of this parameter here. The main results are as follows: For the case  $\epsilon = 0$ ,  $K$  increases slowly and remains close to  $\hbar^2/4$  as

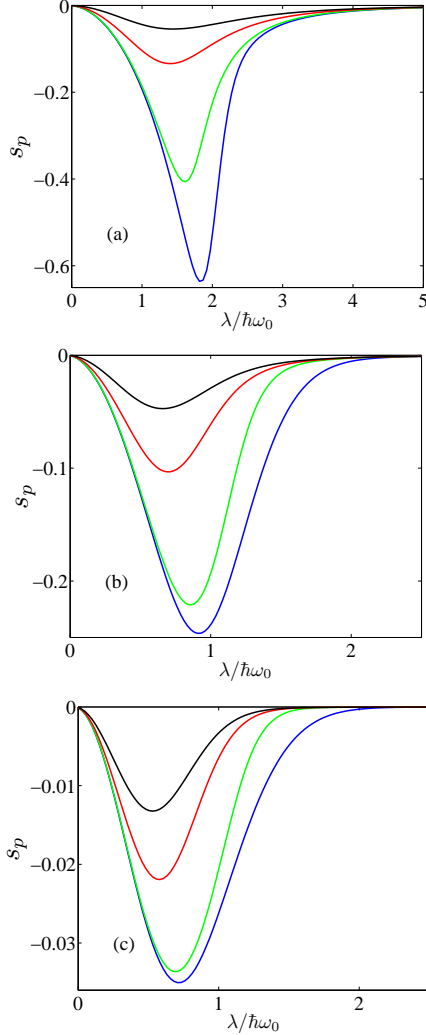


FIG. 8: (Color online) The momentum squeezing parameter  $s_p$  as a function of  $\lambda/(\hbar\omega_0)$  for  $\hbar\omega_0/\Delta = 0.1$  (a), 1 (b) and 10 (c). The different curves correspond to  $\epsilon/\Delta = 0$  (blue), 0.1 (green), 0.5 (red) and 1 (black). The oscillator's state becomes squeezed as the coupling strength  $\lambda$  increases, but then it reaches a maximum and goes back to zero as the qubit and oscillator get entangled in the strong-coupling regime. Note that the maximum achievable squeezing decreases with increasing  $\hbar\omega_0/\Delta$ .

$s_p$  increases, but near the maximum squeezing point,  $K$  starts increasing rapidly and diverges for  $\lambda/(\hbar\omega_0) \rightarrow \infty$ . For finite values of  $\epsilon$ ,  $K$  increases slightly above  $\hbar^2/4$ , but then turns and goes back to  $\hbar^2/4$  as  $s_p$  goes back to zero in the strong-coupling limit.

We have seen that squeezed states are obtained for weak to moderate coupling. The question now is what states we have for strong coupling. The  $Q$ -functions and the  $s_p$  and  $K$  results discussed above do not distinguish between a Schrödinger cat state in the oscillator and a qubit-oscillator entangled state. In order to distinguish between these two possibilities, we now analyze the entanglement properties in the ground state.

The entanglement is quantified by the entropy  $S$  of the qubit's state. This quantity is obtained by calculating the ground state of the combined system  $|\Psi_{GS}\rangle$ , using it to obtain the qubit's reduced density matrix in the ground state  $\rho_q = \text{Tr}_{\text{osc}}\{|\Psi_{GS}\rangle\langle\Psi_{GS}|\}$ , and then evaluating the entropy of that state  $S = -\text{Tr}\{\rho_q \log_2 \rho_q\}$ .

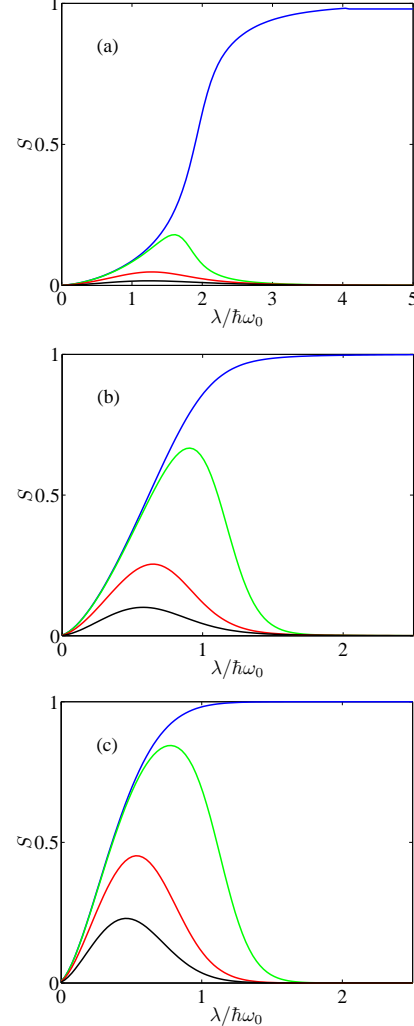


FIG. 9: (Color online) The qubit's entropy (which quantifies the qubit-oscillator entanglement) in the ground state as a function of the coupling strength  $\lambda$ . The ratio  $\hbar\omega_0/\Delta$  is 0.1 in (a), 1 in (b) and 10 in (c), and the different curves in each panel correspond to  $\epsilon/\Delta = 0$  (blue), 0.1 (green), 0.5 (red) and 1 (black). For  $\epsilon = 0$  the qubit-oscillator entanglement increases from zero to one as  $\lambda$  is increased, regardless of the relation between  $\hbar\omega_0$  and  $E_q$ . However, the entanglement drops rapidly (especially for large values of  $\lambda$ ) as  $\epsilon$  is increased, i.e. when the qubit is moved away from the degeneracy point.

In Fig. 9 we plot the qubit's ground-state entropy as a function of  $\lambda$ . For  $\epsilon = 0$  the entropy increases from zero to one as  $\lambda$  is increased from zero to much larger than all other parameters in the problem. Demonstrating the fragility of the entangled states in the large  $\lambda$  limit, Fig. 9 shows that the entanglement drops rapidly (especially for

large values of  $\lambda$ ) when  $\epsilon$  is increased.

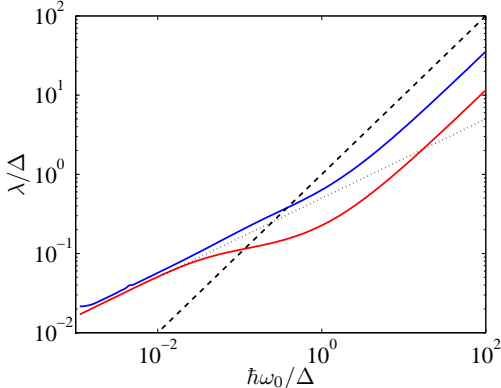


FIG. 10: (Color online) The value of  $\lambda/\Delta$  at which the qubit's ground-state entropy has the values 0.1 (red line) and 0.5 (blue line) plotted as a function of  $\hbar\omega_0/\Delta$  (note the logarithmic scale). Here we take  $\epsilon = 0$ . The straight lines are given by the formulae  $\lambda = \sqrt{\hbar\omega_0 E_q}/2$  (dotted line) and  $\lambda = \hbar\omega_0$  (dashed line), which we have obtained in Sec. III. For small values of  $\hbar\omega_0/\Delta$ , the onset of entanglement occurs when  $\lambda = \sqrt{\hbar\omega_0 E_q}/2$ . For large values of  $\hbar\omega_0/\Delta$ , the onset of entanglement occurs when  $\lambda \sim \hbar\omega_0$ , in agreement with the dependence explained in Sec. III.

In Fig. 10 we examine the value of  $\lambda$  at which the qubit's ground-state entropy has the values 0.1 and 0.5. These curves serve as indicators for the onset of qubit-oscillator entanglement, which is related to the instability encountered in the semi-classical calculation. For a high-frequency qubit, the sharp rise in entanglement occurs at  $\lambda = \sqrt{\hbar\omega_0 E_q}/2$  which agrees with the instability condition of Secs. III C and III D. For a high-frequency oscillator, the sharp rise in entanglement occurs when  $\lambda \sim \hbar\omega_0$ , in agreement with the analysis of Sec. III B.

The rise in the qubit-oscillator entanglement is correlated with the reversal of the squeezing. One therefore goes from a squeezed state in the oscillator to a qubit-oscillator entangled state. We do not find any set of parameters where the ground state contains an unentangled Schrödinger cat state in the oscillator.

The numerical results show that the case  $\hbar\omega_0 \ll E_q$  is most suited for the preparation of squeezed states, as can be seen from the maximum achievable squeezing in the different parameter regimes. The opposite case ( $\hbar\omega_0 \gg E_q$ ) is most suited for the preparation of entangled states, as seen from the extreme fragility of these states for the case  $\hbar\omega_0 \ll E_q$ . In fact, all the non-classical properties of the ground state are suppressed as  $\epsilon$  is increased from zero to values larger than  $\Delta$ . We shall come back to this point in Sec. VI.

## V. PREPARATION AND DETECTION OF NON-CLASSICAL STATES THROUGH *IN-SITU* PARAMETER AND STATE MANIPULATION

We have seen in Sec. IV that oscillator squeezed states and qubit-oscillator entangled states can occur naturally as ground states of the strongly coupled system. Schrödinger-cat states in the oscillator, i.e. not involving entanglement with the qubit, do not occur as ground states of this system.

One method that has been proposed for the generation of oscillator Schrödinger-cat states in the context of cavity QED [2] can be considered here as well: One prepares a qubit-oscillator entangled state of the form

$$\frac{1}{\sqrt{2}} (|q_1\rangle \otimes |\alpha\rangle + |q_2\rangle \otimes |-\alpha\rangle), \quad (35)$$

with  $|q_1\rangle$  and  $|q_2\rangle$  being any two orthogonal qubit states and  $|\pm\alpha\rangle$  are coherent states of the oscillator with a large value of  $|\alpha|$ . This state occurs naturally (to a good approximation) as a ground state in the ultra-strong-coupling regime. One now measures the qubit in the  $(|q_1\rangle \pm |q_2\rangle)/\sqrt{2}$  basis. Depending on the outcome of the measurement, the state of the oscillator is projected into one of the two states

$$\frac{1}{\sqrt{2}} (|\alpha\rangle \pm |-\alpha\rangle), \quad (36)$$

each of which is a Schrödinger-cat state. All three types of non-classical states can therefore be generated in principle.

One important question that arises in the case of strong qubit-oscillator coupling is whether it is possible to detect the non-classical states in spite of the always-present strong coupling. The answer is yes, in principle. Since all of these states occur in the case of a high-frequency, adiabatically adjusting qubit, one can imagine using that regime and at any point in time moving the qubit away from the degeneracy point. This change can be made adiabatic with respect to the qubit but fast with respect to the oscillator. As we have seen in Secs. III and IV, the qubit and oscillator essentially decouple for large values of  $\epsilon$ , and such a bias point can be used during the detection stage of the experiment.

The state of the oscillator can be reconstructed using Wigner tomography, which could be implemented following the experiment in Ref. [12]. In the case of a low-frequency oscillator, the transfer of excitations between the qubit and the oscillator can be induced by driving the red or blue sideband, as was done in the experiment of Ref. [4]. Since, as explained above, the qubit is effectively decoupled from the resonator when  $\epsilon \gg \Delta$ , a second weakly coupled qubit could be used for measurement purposes. Wigner tomography can be used to demonstrate squeezed and Schrödinger-cat states in the oscillator. Qubit-oscillator entangled states could be demonstrated indirectly following the cat-state-preparation scheme explained above: Successful preparation of the cat state

would serve as evidence that the initial state was indeed the theoretically predicted entangled state.

## VI. DECOHERENCE

We have considered the possibility of preparing non-classical states by letting the system cool down to a ground state with non-classical properties. One important parameter in this context is the ambient temperature of the system. In superconducting circuits, the temperature is typically around 20 mK, which can be converted to roughly 1 GHz in frequency units. The ground state must be separated from the excited states by at least that amount in order to achieve high-fidelity preparation of the ground state. Typical qubit and oscillator frequencies are in the few-gigahertz range, not much higher than typical temperatures. Squeezed ground states in the oscillator should be separated from the excited states by an energy comparable to the one present in the uncoupled system, implying that the preparation of these states should be possible. The Schrödinger-cat ground states discussed in Sec. IV, however, are separated from the first excited states by energy gaps that decrease rapidly with increasing qubit-oscillator coupling strength. If this energy gap becomes smaller than the 1 GHz temperature level, one would not be able to prepare the system in the ground state. Lower temperatures should be achievable with current technology, and the above limit should not be seen as a fundamental obstacle, even though it might be a serious limiting factor for present experimental setups.

As mentioned in the introduction, the availability of the tuning parameter  $\epsilon$  can be seen as an advantage of solid-state qubits in comparison to natural atoms in cavity QED. On the other hand, this property also opens a new channel for noise and the environment to couple to the system. As a result, entangled states can be fragile against decoherence, especially for very strong coupling, where the energy separation between the ground state and first excited state becomes very small.

The most serious effect of the environment on the qubit is the tendency for the environment to localize the qubit in one of the eigenstates of  $\hat{\sigma}_z$ , since this is the operator through which the qubit couples to the environment. An important parameter here is the qubit's dephasing time when biased away from the degeneracy point. This parameter is typically of the order of 10 ns, giving a dephasing rate of 100 MHz. The qubit is protected from this noise at the degeneracy point, because the qubit's gap is typically larger than 1 GHz at the degeneracy point, where the qubit-environment coupling is transverse to the qubit Hamiltonian. Since entangled ground states are separated from the first excited states by a very small energy, no protection of the degeneracy-point type will suppress the 100 MHz decoherence rate. This decoherence rate must therefore be reduced, and in principle this should be possible in the future using better materials

and circuit designs.

Even though superconducting harmonic oscillators generally have much higher quality factors than superconducting qubits, it is instructive to briefly discuss the effect of oscillator decoherence. The oscillator couples to its environment through the operator  $\hat{x}$ , or equivalently  $\hat{a} + \hat{a}^\dagger$ . In a free oscillator at low temperatures, the effect of the environment is to cause decay to the ground state through the loss of photons. This process is described by the jump operator  $\hat{a}$  and occurs with a rate that is proportional to the environment's power spectrum at the oscillator frequency. In the strongly-coupled qubit-oscillator system with the double-well effective potential, the effect of the environment will be drastically different. Since the effective potential has the same shape as the free-oscillator potential, the coupling to the environment should cause decay in the two wells with a rate equal to the free-oscillator decay rate (note that this process is no longer described by the operator  $\hat{a}$ , but rather by a properly shifted annihilation operator). The coupling to the environment will also cause dephasing in any quantum superposition involving the two wells. The rate of this process will be proportional to the product of the environment's power spectrum at zero frequency and the quantity  $|\langle \psi_R | (\hat{a} + \hat{a}^\dagger) | \psi_R \rangle|^2 - |\langle \psi_L | (\hat{a} + \hat{a}^\dagger) | \psi_L \rangle|^2$  for the two states localized in the left and right wells [25]. This last quantity is proportional to  $x_0$  of Sec. III C, and it grows indefinitely with increasing coupling strength. If we assume that the power spectrum at zero frequency is comparable to that at the oscillator frequency, this dephasing rate can be much larger than the decay rate of the free oscillator because of the largeness of the quantity  $|\langle \psi_R | (\hat{a} + \hat{a}^\dagger) | \psi_R \rangle|^2 - |\langle \psi_L | (\hat{a} + \hat{a}^\dagger) | \psi_L \rangle|^2$ .

## VII. CONCLUSION

We have analyzed the properties of a strongly coupled qubit-oscillator system, focusing on the potential of this system for the preparation of non-classical states. We have compared the predictions of a number of analytical methods that can be used to describe the system under a number of different assumptions, thus covering a number of different parameter regimes. We have then presented results of numerical calculations that demonstrate the non-classical properties of the energy eigenstates, and especially the ground state, of the system. We have shown that non-classical states, particularly highly-entangled states, are highly susceptible to fluctuations in the bias parameters. These results lead to the conclusion that high degrees of control and low noise levels will be required for the preparation of robust non-classical states in the case of ultra-strong coupling.

This work was supported in part by the National Security Agency (NSA), the Army Research Office (ARO), the Laboratory for Physical Sciences (LPS) and the National Science Foundation (NSF) grant No. 0726909.

---

[1] E. T. Jaynes and F. W. Cummings, Proc. IEEE **51**, 89 (1963).

[2] See e.g. C. C. Gerry and P. L. Knight, *Introductory Quantum Optics* (Cambridge University Press, 2005); D. F. Walls and G. J. Milburn, *Quantum Optics* (Springer, Berlin, 1994); M. O. Scully and M. S. Zubairy, *Quantum Optics* (Cambridge University Press, 1997).

[3] H. J. Kimble, Phys. Scr. **T76**, 127 (1998); J. M. Raimond, M. Brune, and S. Haroche, Rev. Mod. Phys. **73**, 565 (2001); S. Haroche and J. M. Raimond, *Exploring the Quantum: Atoms, Cavities, and Photons* (Oxford University Press, 2006).

[4] I. Chiorescu, P. Bertet, K. Semba, Y. Nakamura, C. J. P. M. Harmans, J. E. Mooij, Nature **431**, 159 (2004).

[5] A. Wallraff, D. I. Schuster, A. Blais, L. Frunzio, R.-S. Huang, J. Majer, S. Kumar, S. M. Girvin, R. J. Schoelkopf, Nature **431**, 162 (2004).

[6] For recent reviews on superconducting qubit circuits, see e.g. J. Q. You and F. Nori, Phys. Today **58** (11), 42 (2005); G. Wendin and V. Shumeiko, in *Handbook of Theoretical and Computational Nanotechnology*, ed. M. Rieth and W. Schommers (ASP, Los Angeles, 2006); R. J. Schoelkopf and S. M. Girvin, Nature, **451**, 664 (2008); J. Clarke and F. K. Wilhelm, Nature **453**, 1031 (2008).

[7] K. Hennessy, A. Badolato, M. Winger, D. Gerace, M. Atatüre, S. Gulde, S. Fält, E. L. Hu, and A. Imamoglu, Nature (London) **445**, 896 (2007).

[8] R. Leturcq, C. Stampfer, K. Inderbitzin, L. Durrer, C. Hierold, E. Mariani, M. G. Schultz, F. von Oppen, and K. Ensslin, Nat. Phys. **5**, 327 (2009); M. D. LaHaye, J. Suh, P. M. Echternach, K. C. Schwab, and M. L. Roukes, Nature **459**, 960 (2009); G. A. Steele, A. K. Hüttel, B. Witkamp, M. Poot, H. B. Meerwaldt, L. P. Kouwenhoven, and H. S. J. van der Zant, Science **325**, 1103 (2009).

[9] A. D. Armour, M. P. Blencowe, and K. C. Schwab, Phys. Rev. Lett. **88**, 148301 (2002).

[10] T. Holstein, Ann. Phys. (N.Y.) **8**, 325 (1959).

[11] W. D. Oliver, Y. Yu, J. C. Lee, K. K. Berggren, L. S. Levitov, T. P. Orlando, Science **310**, 1653 (2005).

[12] M. Hofheinz, E. M. Weig, M. Ansmann, R. C. Bialczak, E. Lucero, M. Neeley, A. D. O'Connell, H. Wang, J. M. Martinis, and A. N. Cleland, Nature **454**, 310 (2008); M. Hofheinz, H. Wang, M. Ansmann, R. C. Bialczak, E. Lucero, M. Neeley, A. D. O'Connell, D. Sank, J. Wenner, J. M. Martinis and A. N. Cleland, Nature **459**, 546 (2009).

[13] See also D. I. Schuster, A. A. Houck, J. A. Schreier, A. Wallraff, J. M. Gambetta, A. Blais, L. Frunzio, J. Majer, B. R. Johnson, M. H. Devoret, S. M. Girvin, and R. J. Schoelkopf, Nature **445**, 515 (2007).

[14] F. G. Paauw, A. Fedorov, C. J. P. M. Harmans, and J. E. Mooij, Phys. Rev. Lett. **102**, 090501 (2009).

[15] M. H. Devoret, S. Girvin and R. Schoelkopf, Ann. Phys. **16**, 767 (2007).

[16] A. P. Hines, C. M. Dawson, R. H. McKenzie, and G. J. Milburn, Phys. Rev. A **70**, 022303 (2004); C. P. Meaney, T. Duty, R. H. McKenzie, and G. J. Milburn, arXiv:0903.2681.

[17] E. K. Irish, J. Gea-Banacloche, I. Martin, and K. C. Schwab, Phys. Rev. B **72**, 195410 (2005); E. K. Irish, Phys. Rev. Lett. **99**, 173601 (2007).

[18] J. Larson, Phys. Scr. **76**, 146 (2007); arXiv:0804.4416; arXiv:0908.1717.

[19] D. Zueco, G. M. Reuther, S. Kohler, and P. Hänggi, Phys. Rev. A **80**, 033846 (2009).

[20] I. Lizuain, J. Casanova, J. J. Garcia-Ripoll, J. G. Muga, and E. Solano, arXiv:0912.3485.

[21] For recent proposals for the generation of squeezed and Schrödinger-cat states in superconducting resonators, see e.g. Y.-X. Liu, L.-F. Wei, and F. Nori, Europhys. Lett. **67**, 941 (2004); Phys. Rev. A **71**, 063820 (2005); M. Mariantoni, F. Deppe, A. Marx, R. Gross, F. K. Wilhelm, and E. Solano, Phys. Rev. B **78**, 104508 (2008); A. M. Zagoskin, E. Illichev, M. W. McCutcheon, J. F. Young, and F. Nori, Phys. Rev. Lett. **101**, 253602 (2008).

[22] J. Bourassa, J. M. Gambetta, A. A. Abdumalikov, O. Astafiev, Y. Nakamura, and A. Blais, Phys. Rev. A **80**, 032109 (2009).

[23] B. Peropadre, P. Forn-Diaz, E. Solano, and J. J. Garcia-Ripoll, arXiv:0912.3456.

[24] M. A. Sillanpää, T. Lehtinen, A. Paila, Yu. Makhlin, L. Roschier, and P. J. Hakonen, Phys. Rev. Lett. **95**, 206806 (2005); T. Duty, G. Johansson, K. Bladh, D. Gunnarsson, C. Wilson, and P. Delsing, Phys. Rev. Lett. **95**, 206807 (2005); G. Johansson, L. Tornberg, and C. M. Wilson, Phys. Rev. B **74**, 100504(R) (2006).

[25] See e.g. C. Cohen-Tannoudji, J. Dupont-Roc, and G. Grynberg, *Atom-Photon Interactions* (Wiley, New York, 1992).